Modeling of a twisted kagome HoAgGe spin ice using reduced configuration space search and density functional theory

Gunnar F. Schwertfeger, Po-Hao Chang, Predrag Nikolić, and Igor I. Mazin
Department of Physics and Astronomy, George Mason University, Fairfax, Virginia 22030, USA
and Quantum Science and Engineering Center, George Mason University, Fairfax, Virginia 22030, USA

(Received 21 July 2025; accepted 28 October 2025; published 5 December 2025)

The kagome lattice is a two-dimensional (2D) network of corner-sharing triangles found in several rare-earth materials resulting in a complicated and often frustrated magnetic system. In the past decades, modifications of the motif, such as breathing kagome, asymmetric kagome, and twisted kagome, were brought into the limelight. In particular, the latter has symmetry lower than that of the original kagome and thus allows implementations of an "Ising-local" Hamiltonian, leading to a 2D spin ice. One such material implementation, HoAgGe, was recently reported to have an exceptionally rich phase diagram and is a strongly frustrated 2D spin-ice material with a twisted kagome geometry. In the presence of an external magnetic field the compound exhibits steplike magnetization plateaus at simple fractions of the saturation magnetization. It is believed that this phenomenon results from strong single-site anisotropy, which in HoAgGe was found to be in-plane and along a high-symmetry direction. Previous Monte Carlo simulations with empirical exchange parameters explain some, but not all, experimental observations. In this work, we present (a) first-principles calculations of the crucial model parameters and (b) direct energy minimization via a reduced configuration space search, as well as Monte Carlo simulations of the field-dependent phase diagram. We find that for HoAgGe the calculated exchange parameters are very different from the earlier suggested empirical ones, and we describe the phase diagram much more accurately. This is likely because the first-principles parameters are, in addition to geometrically, also parametrically frustrated.

DOI: 10.1103/p8bq-9623

I. INTRODUCTION

Magnetic frustration has been the source of many exotic phenomena in matter. In three-dimensional (3D) rare-earth pyrochlore compounds, for instance, one finds a rather unique phenomenon dubbed "spin ice" [1]. In a new twist, a two-dimensional (2D) material, HoAgGe, was recently reported [2] to be an example of 2D spin ice. Spin ice is, typically, a highly frustrated magnetic system where each magnetic site has a strong uniaxial anisotropy, with the axis varying from site to site according to the crystal symmetry.

The kagome lattice is formed from corner-sharing equilateral triangles (Fig. 1). As the kagome lattice is the 2D analog of the 3D pyrochlore lattice, it is natural to look for spin-ice behavior there. In the last decades, various interesting modifications of the kagome lattice have also been discussed in the literature, such as breathing kagome [3], distorted kagome [4], square kagome [5], etc. One of the newest developments is the so-called [6] twisted kagome lattice, where the alternating triangles in the lattice are twisted around their centers in the opposite directions. This operation lowers the symmetry from $P6mmm$ to $P\bar{6}/2m$. In particular, the site symmetry is lowered from mmm to $m2m$, as one can see from Fig. 1, and the global inversion symmetry is also lost.

The recently reported magnetic compound HoAgGe [2] has this twisted kagome structure, with the twisting angle $\sim 15.6^\circ$ (again as depicted in Fig. 1). Ho^{3+} atoms in this compound have ten f-electrons, a large orbital moment, and strong spin-orbit coupling. Therefore, the single-site anisotropy is large and, generally speaking, can have any easy axis, in or out of plane [7]. Experimental evidence suggests that the easy axis for Ho is along a high-symmetry direction as indicated by the arrows in Fig. 1. Our first-principles calculations described below confirm this.

In this case, the magnetic Hamiltonian, to a good approximation, is local Ising, in the sense that each spin can assume only two directions. This results in a "two-in-one-out" spin-ice rule in plane for the triangular nearest-neighbor interactions between Ho atoms in the twisted kagome lattice. This is analogous to the "two-in-two-out" rule observed in the tetrahedra in pyrochlore spin-ice compounds [1]. Existing experimental data are reasonably well consistent with this picture [2,8] (albeit small, but distinct deviations from the infinite-anisotropy model were reported in Ref. [8]). As the dominant interaction is antiferromagnetic, the ground state in zero field has zero magnetization, and the spins form a $\sqrt{3} \times \sqrt{3}$ supercell, as depicted in Fig. 6, with the magnetic space group retaining the hexagonal symmetry $P\bar{6}'m2'$. In the in-plane saturation field, whose value depends on the field direction, all spins assume the direction most parallel to the applied field.

Experimentally, the "iceness" of the system is reflected in the multiple magnetization steps in an in-plane magnetic field $\mathbf{h}$. Indeed, HoAgGe exhibits, in an external magnetic field, several of these unique magnetic steps. These steps are simple fractions of the total magnetization. While some of the

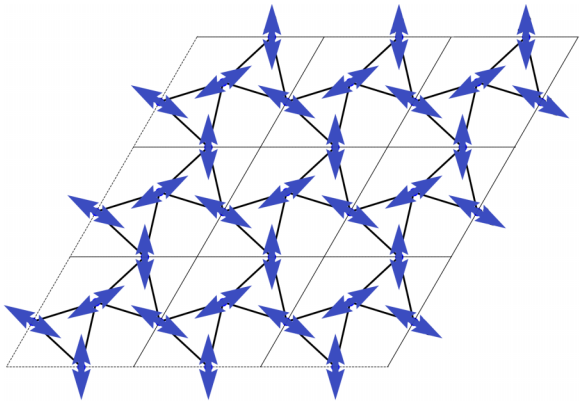

FIG. 1. Twisted kagome lattice with J_1 bonds visualized (a 3×3 supercell is shown). The arrows indicate the easy axis in HoAgGe.

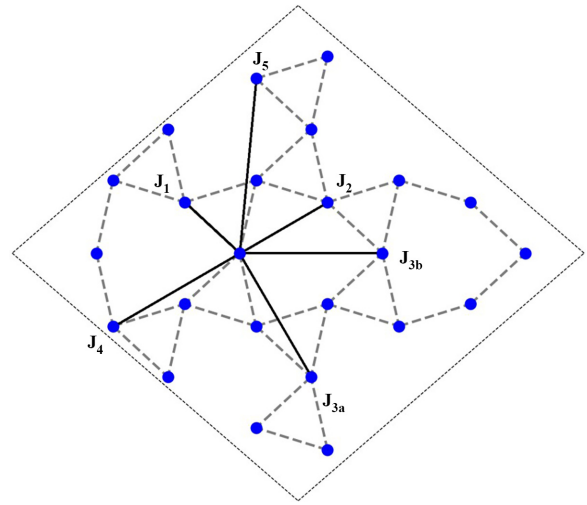

FIG. 2. Nearest-neighbor exchange interactions, J_1 to J_5, depicted for a single atom.

larger steps (such as the 1/3 and 2/3 magnetization plateaus observed for $\mathbf{h}||y$) have been explained in earlier works [2], many smaller magnetization steps, particularly those observed for $\mathbf{h}||x$, have not been explained.

To this end, we have, first, performed first-principles DFT + U calculations, making sure that the Hund's rule on Ho is respected [7,9], as discussed below, and extracted six Heisenberg exchange parameters, up to the fifth nearest neighbors (as opposed to three parameters used in the empirical model of Ref. [2]). The resulting parameters are completely different from the latter, yet provide a better description of experimentally observed plateaus not only for $\mathbf{h}||y$, but also for $\mathbf{h}||x$. Using these parameters, we constructed full-exchange Hamiltonians [as discussed below, the Dzyaloshinskii-Moriya and dipole-dipole interactions appear to be not important] and directly minimized the energy by performing a search over a reduced configuration space for all possible supercells up to 18 formula units and constructed the zero-temperature phase diagram for both field directions. We found that all major phases are very stable, and secondary phases, corresponding to smaller magnetization plateaus, are on the borderline of stability, but still present. Thus, we identified all nine experimentally observed phases. To further validate the experimentally determined local easy-axis orientation, we also performed total energy calculations comparing several in-plane spin configurations (see Supplemental Material [10]). These calculations confirm that the local easy axis for Ho lies along a high-symmetry direction, as indicated in Fig. 1.

In addition, we attempted Monte Carlo simulations similar to those in Ref. [2], but, as opposed to their model, our calculated Hamiltonian is much more frustrated, so finding the global energy minimum in MC calculations is challenging.

II. GENERAL MODEL

A. Crystal lattice Hamiltonian

The Hamiltonian for the spin-ice crystal HoAgGe is

$$H[M; J_\alpha, h] = -\sum_\alpha J_\alpha \sum_{\langle i,j\rangle_\alpha} \hat{\mathbf{S}}_i \cdot \hat{\mathbf{S}}_j - h \sum_i \hat{\mathbf{S}}_i \cdot \hat{\mathbf{h}}, \quad (1)$$

where $M = \{\hat{\mathbf{S}}_0, \hat{\mathbf{S}}_1, \ldots, \hat{\mathbf{S}}_N\}$ defines a particular state of the crystal lattice, J_α are Heisenberg exchange parameter, and h is the applied magnetic field along $\hat{\mathbf{h}}$. All spins, $\hat{\mathbf{S}}_i$ and $\hat{\mathbf{h}}$ are unit length vectors in $\mathbb{R}^3$. Here, i and j label lattice sites, and α enumerates the Ho-Ho bonds of different lengths on which two spins interact (shown in Fig. 2). Again, as the Ho atoms have large magnetic moments, we can treat these spins classically.

Using a method described in a previous paper by some of us [11], we considered periodic magnetic orders as ground-state candidates, with tessellating supercells of various sizes and shapes. A supercell effectively has periodic boundary conditions; if a supercell is very small, then a long-range exchange parameter doubles back on the same supercell atom, which results in a constant positive addition to the lattice energy per antiferromagnetic pair or a constant negative addition per ferromagnetic pair. However as we search supercells containing up to octodecuple ($\times 18$) Ho atoms, all six exchange parameters play nontrivial roles.

Exchange interactions are defined by their relative distances and crystallographic symmetry. For J_1, J_2, J_4, and J_5, it is enough to use only the corresponding bond lengths to distinguish interaction types. However, for J_3 we have elected to divide these interactions further into crystallographically inequivalent J_{3a} and J_{3b} (in Ref. [2] they were assumed to be equal; however, there is no microscopic justification for that).

Atoms joined by J_2, J_4, or J_5 couplings also satisfy the two-in-one-out spin-ice rule, further compounding the system's frustration. This is particularly true in the case of J_5 interactions because, like the nearest neighbor J_1, neighboring J_5 pairs also form corner-sharing triangles between atoms. These interactions form decoupled lattices, each still obeying the spin-ice rule between triangles of interacting atoms.

By finding the lattice configurations which minimize Eq. (1) for particular values of J_α and h, the magnetic plateaus observed experimentally should be reproduced given a sufficiently large maximum magnetic unit cell.

For a particular super cell of N atoms, if each atom is in one of q possible states, the total number of configurations of the supercell is simply q^N, meaning the total number of elements in the configuration space $\mathbb{M}$ is finite. On sufficiently small

lattices with up to $N = 18$ sites, one formally can generate every possible spin configuration and check their energy, but the number of configurations grows exponentially with system size. Using Eq. (1), however, we can greatly reduce the number of states in $\mathbb{M}$ that need to be considered by eliminating symmetrically equivalent states.

For any particular state $M \in \mathbb{M}$, we define the constants $C_\alpha[M]$ and $\langle M\rangle_i$ using Eqs. (2) and (3):

$$C_\alpha[M] = \sum_{\langle i,j\rangle_\alpha} \hat{\mathbf{S}}_i \cdot \hat{\mathbf{S}}_j, \tag{2}$$

$$\langle M\rangle_i = \sum_j \hat{\mathbf{S}}_j \cdot \hat{\mathbf{e}}_i, \tag{3}$$

Using Eq. (1), the Hamiltonian for any given state may be written as Eq. (4):

$$H_M[J_\alpha, h] = -\sum_\alpha J_\alpha C_\alpha - \sum_i h_i \langle M\rangle_i, \tag{4}$$

meaning each Hamiltonian for a state in $\mathbb{M}$ can be characterized by $\alpha + 3$ parameters. By collecting only the states which exhibit unique values for C_α and $\langle M\rangle_i$ and therefore by Eq. (4) constitute a unique Hamiltonian, the total number of unique states of the supercell is greatly diminished. Meaning the search over configuration space for the lowest energy state for any combination of J_α and h is significantly reduced. For this reason, we refer to this method as a reduced configuration space search (RCS search).

B. Magnetic dipole interaction

In principle, in rare-earth systems the magnetic dipole-dipole interactions may be relevant; they can be introduced to the Hamiltonian as follows:

$$E_{dd} = -\frac{g_{dd}}{|\vec{\mathbf{r}}_{ij}|^3}[3(\hat{\mathbf{S}}_i \cdot \hat{\mathbf{r}}_{ij})(\hat{S}_j \cdot \hat{\mathbf{r}}_{ij}) - (\hat{\mathbf{S}}_i \cdot \hat{\mathbf{S}}_j)],$$

$$g_{dd} = \frac{\mu_0 \mu_B^2 g^2}{4\pi},$$

$$\langle E_{dd}\rangle = \sum_{\alpha,\langle i,j\rangle_\alpha} \frac{[3(\hat{\mathbf{S}}_i \cdot \hat{\mathbf{r}}_{ij})(\hat{\mathbf{S}}_j \cdot \hat{\mathbf{r}}_{ij}) - (\hat{\mathbf{S}}_i \cdot \hat{\mathbf{S}}_j)]}{|\vec{\mathbf{r}}_{ij}|^3},$$

$$H_M[J_\alpha, h, g_{dd}] = -\sum_\alpha J_\alpha C_\alpha - \sum_i h_i \langle M\rangle_i - g_{dd}\langle E_{dd}\rangle. \tag{5}$$

An additional term to the Hamiltonian means that each Hamiltonian is now characterized by $\alpha + 4$ parameters and when searching through all forms of M in $\mathbb{M}$ some degeneracies may be lifted, allowing for more unique Hamiltonians to be observed. Using a g-factor of 10 (as was reported in Ref. [2]), g_{dd} is calculated to be 5.3681 meV Å^3. With the distance between nearest-neighbor Ho-Ho atoms of 3.67 Å, the dipole-dipole interaction is estimated to have an average energy of -0.1085 meV, far below the J_1 interaction energy of 3.154 meV. While this may initially appear negligible, especially when an external magnetic field is applied to the crystal, the minute effect of the dipole interaction is critical in distinguishing between potential states that are extremely close in energy.

C. Dzyaloshinskii-Moriya interaction (DMI)

As the twisted kagome lattice of the HoAgGe crystal is two dimensional with the XY plane being a mirror plane for the lattice, it is easy to determine the unit DMI vector $\hat{\mathbf{D}}_{ij}$ for the nearest-neighbor interactions to be aligned perpendicular to the plane along the $\pm\hat{\mathbf{z}}$ direction. Through further symmetry considerations, it is then possible to determine the orientation of the $\hat{\mathbf{D}}_{ij}$ vector for each interaction.

In a similar fashion as was done to include the contribution of the dipole interaction, to account for the energy contribution to the Hamiltonian from the DMI we must introduce an additional term, B_α, to the Hamiltonian of Eq. (4). We can then define the DMI scalar D_α, similar to the Heisenberg exchange parameters.

$$B_\alpha[M] = \sum_{\langle i,j\rangle_\alpha} (\hat{\mathbf{S}}_i \times \hat{\mathbf{S}}_j) \cdot \hat{\mathbf{D}}_{ij},$$

$$H_M[J_\alpha, D_\alpha, h, g_{dd}] = -\sum_\alpha (J_\alpha C_\alpha + D_\alpha B_\alpha) - \sum_i h_i \langle M\rangle_i - g_{dd}\langle E_{dd}\rangle. \tag{6}$$

With the introduction of additional parameters to the Hamiltonian, even more degeneracy is expected to be lifted. However, in this particular case, as the magnetic moments of each Ho atom are either at $2\pi/3$ rad or parallel to all other neighboring moments, the Dzyaloshinskii-Moriya interactions simplify into a scalar of the corresponding Heisenberg interaction and may safely be absorbed into the exchange parameter J_α. This is confirmed through direct calculation as for all allowed supercell Hamiltonians for the Ho lattice, $B_\alpha = \sqrt{3}C_\alpha$.

D. Calculation of exchange parameters

The calculations described below have been, to a large part, described in an earlier paper [8], but we briefly outline them below for completeness. A numerical-orbital-based [12] DFT code openmx [13] was first used to obtain the ground-state Hamiltonian. The Perdew-Burke-Enzerhof [14] generalized gradient approximation was employed to describe exchange-correlation effects. To ensure the proper f-shell occupation, a large Hubbard U correction is used to account for the strongly correlated Ho $4f$ states [15,16] (since these states are well removed from the Fermi level, the exact value of U in this case is not important, as compared to d metals). The exchange coupling constants are then calculated perturbatively using Green's function (GF) method [17,18] implemented in openmx 3.9 [19,20]. Calculated exchange parameters are compared with exchange parameters assumed by Zhao *et al* [2] in Table I.

III. ANALYSIS OF HoAgGe MODEL

A. Average magnetization

The minimum antiferromagnetic supercell is the $\sqrt{3} \times \sqrt{3}$ supercell (Fig. 3 red). Using this supercell and imposing periodic boundary conditions gives a system of nine atoms with each atom in one of the two states. There are then $2^9 = 512$

TABLE I. The comparison between the effective exchange coupling constants up to the fourth nearest neighbor assumed by Zhao *et al.* [2] and up to the fifth nearest neighbor calculated using DFT and GF. The values of the former are normalized to $J_1 = 2$ meV and the latter are normalized to $J_1 = 3.154$ meV. NN here is the coordination number of the corresponding bond. Note that in Ref. [2], J_{3a}, J_{3b}, and J_4 were assumed to be equal.

		Ref. [2]	DFT-GF
	NN	$J_\alpha/\lvert J_1\rvert$	
J_1	4	1	1
J_2	2	−0.115	−0.442
J_{3a}	4	−0.064	−0.131
J_{3b}	2	−0.064	−0.175
J_4	2	−0.064	−0.023
J_5	4		−0.067

total elements in the configuration space, meaning 512 possible states can be represented on the $\sqrt{3} \times \sqrt{3}$ supercell. However, the number of states with unique Hamiltonians is only 88. These states are then compared to find the lowest-energy configuration as the applied magnetic field is increased.

This is done for all possible guesses of magnetic unit cells with the volume less than or equal to six times the volume of a single unit cell. This gives 3540 acceptable supercells. The states that exhibit unique Hamiltonians are then compared against each other to create a list of 220 170 states with unique Hamiltonians covering 33 possible supercell shapes. Of those, only 6 shapes appear to be relevant to minimum-energy states for any in-plane field. These shapes are shown in Fig. 3.

Using the exchange parameters conjectured by Zhao *et al.* [2] and applying the above protocol, the resulting average magnetization of the minimum energy states can then be directly compared with the experiment in Fig. 4. Note again that there is no distinction between bonds of types J_{3a} and J_{3b} for their set of parameters.

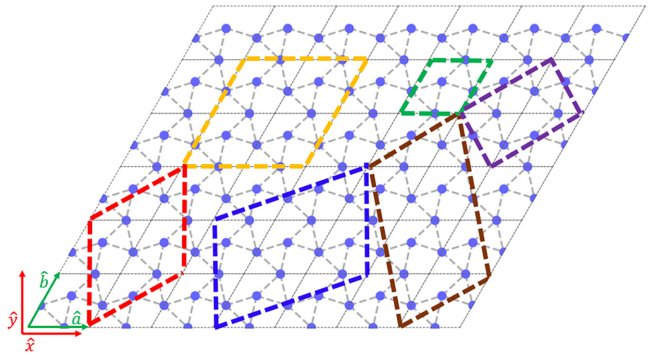

FIG. 3. Magnetic supercells exhibiting the lowest energy for different in-plane fields: the 1×1 supercell (green), the $\sqrt{3} \times 1$ supercell (purple), the $\sqrt{3} \times \sqrt{3}$ supercell (red), the 2×2 supercell (yellow), the $\sqrt{3} \times \sqrt{7}$ supercell (brown), and the $\sqrt{7} \times \sqrt{3}$ supercell (blue). Unit vectors $\hat{x}$, $\hat{y}$, $\hat{a}$, and $\hat{b}$ are included for reference clarity.

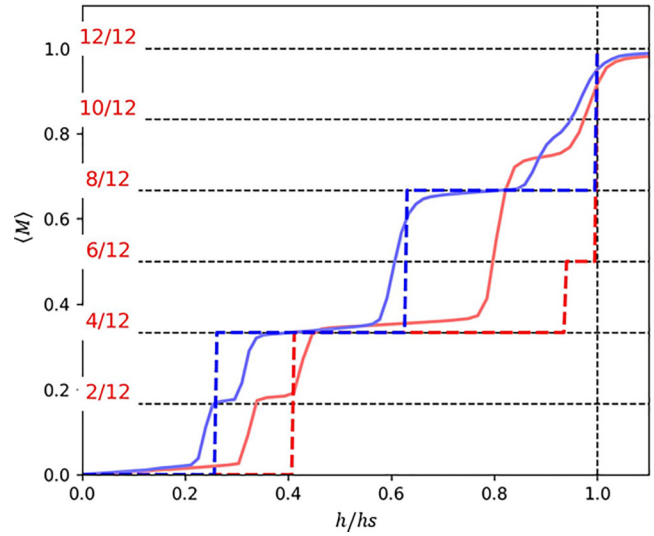

FIG. 4. Average Ho^{3+} magnetization as an external magnetic field is applied perpendicular (X, red) and parallel (Y, blue) to the easy axis as found by direct minimization and empirical exchange parameters of Ref. [2] (dashed lines), compared to experiment [8].

While the resulting magnetization curves (dashed) do represent, to some extent, experimental measurements (specifically the two most prominent magnetization plateaus at the 1/3 and 2/3 magnetizations), this Hamiltonian does not fully describe the experiment.

Using the other set of exchange parameters, calculated, as described, using DFT-GF method, the same states can again be analyzed with new parameters and the total magnetization is plotted in Fig. 5.

Importantly, this set of parameters distinguishes between J_{3a} and J_{3b} while including the further neighbor coupling parameter J_5. For this reason, the calculated values of J_α

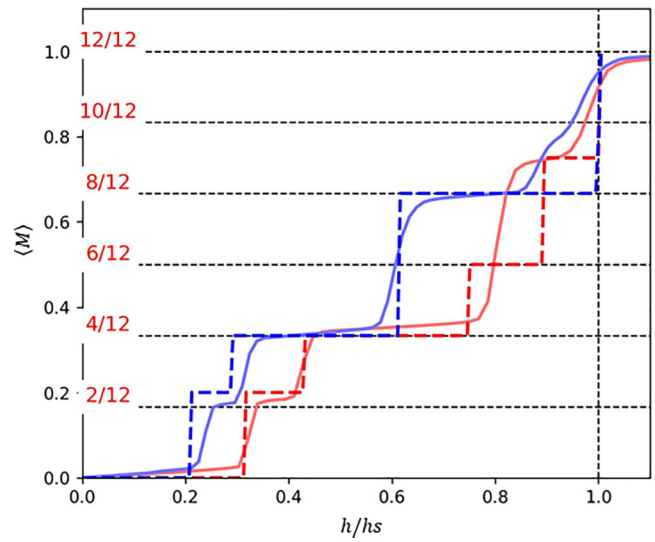

FIG. 5. Average Ho^{3+} magnetization as an external magnetic field is applied perpendicular (X, red) and parallel (Y, blue) to the easy axis found using direct minimization and our calculated DFT-GF exchange parameters (dashed lines) compared to experiment [8].

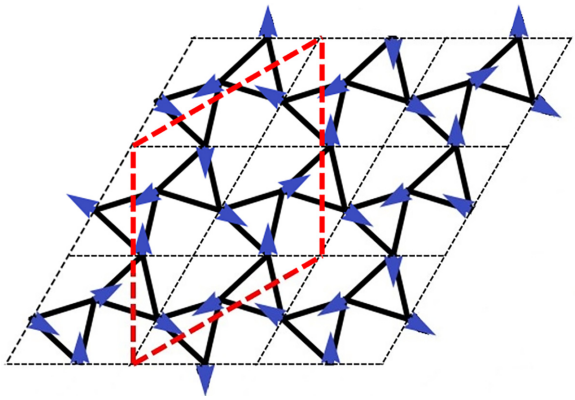

FIG. 6. The ground-state $\sqrt{3} \times \sqrt{3}$ supercell (red) with magnetic space group $P\bar{6}'m2'$.

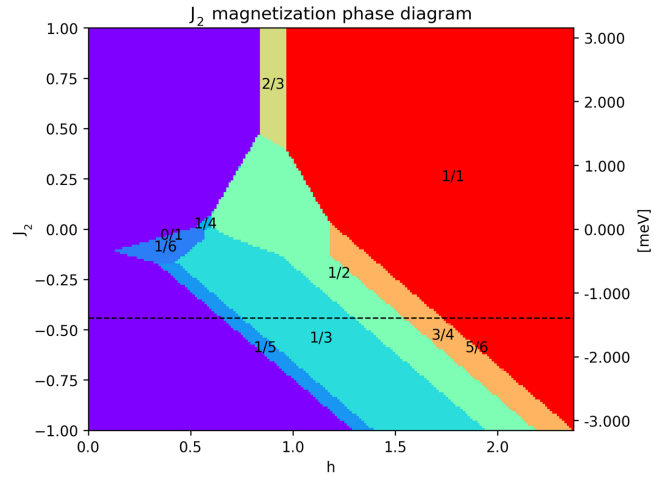

FIG. 7. J_2 Magnetic phase diagram for a magnetic field applied in the X direction. Colors represent average magnetization in the X direction. The dotted line is the theorized value for J_2. Again, all interactions are normalized to $J_1 = 3.154$ meV.

appear significantly different than those found empirically but still describe the system sufficiently. In fact, these inclusions significantly improve the accuracy of the model, particularly in the X direction, perpendicular to the easy axis of the Ho atoms.

Surprisingly, what was initially assumed to be a small $1/6$ magnetic plateau is not directly observed using this method. However, a $1/5$ magnetization state is observed. These new parameters exhibit several small steps between the larger $1/3$ and $2/3$ states and the fully saturated state plateaus. These are the $1/5$, $1/2$, and $3/4$ states. These states were not observed using the empirical parameters, but are observed experimentally. In total, the inclusion of the further nearest neighbor, J_5, and distinguishing between J_{3a} and J_{3b} type interactions resulted in ten distinct magnetization steps [21] again defined by the six shaped cells shown in Fig. 3. The inclusions of further neighbor interactions, J_5, does not generate significant change for magnetic fields applied in the Y direction, but still describe the magnetic behavior as accurately as the empirical parameters, even finding the same ground state (Fig. 6).

It should be noted that for the ground state, in particular, there are several states [22] we find to be exceptionally close in energy. Among the potential minimum energy states found using this method was the previously found HoAgGe magnetic ground state. So while we find several other states with similar energy, as the previously reported state was the only configuration of the correct magnetic space group, this is in agreement within the accuracy of our model. Any further degeneracy between these states may potentially be lifted through the employment of further neighbor interactions.

In total, using a RCS Search method, we found the ground state and all major magnetization steps observed in experiment (0, $1/5(x)$, $1/5(y)$, $1/3(x)$, $1/3(y)$, $2/3(y)$, $3/4(x)$, $1(x)$, and $1(y)$. Shown in Supplemental Material [10]). Among them, all states previously found empirically in Ref. [2] were again seen and confirmed using this method.

B. J_α-h phase diagrams and minimum-energy curves

Using this procedure, it is relatively simple to vary the parameters J_α and h and search for which Hamiltonian of which magnetic unit cell has the lowest energy. By repeating this process and varying any one J_α, phase diagrams of the system's behavior can be produced. As all exchange parameters are normalized to the nearest neighbor J_1, we calculate the phase diagrams for all interactions other than the first. This allows a visual inspection for the stability against any of these parameters and the behavior of the model. The resulting J_2 phase diagram for a field applied in the X direction is shown in Fig. 7. From inspecting the remaining J_{3a}, J_{3b}, J_4, and J_5 magnetic phase diagrams [23], for fields applied in the X direction in particular, it is clear that almost no adjustments can easily be made to the internal coupling parameters without seriously altering the behavior of the model, in some cases introducing new magnetic plateaus and in other cases removing steps.

The close competition between states can be seen directly in Fig. 8 as many states of different shapes and magnetization are found to be close in energy, especially near phase

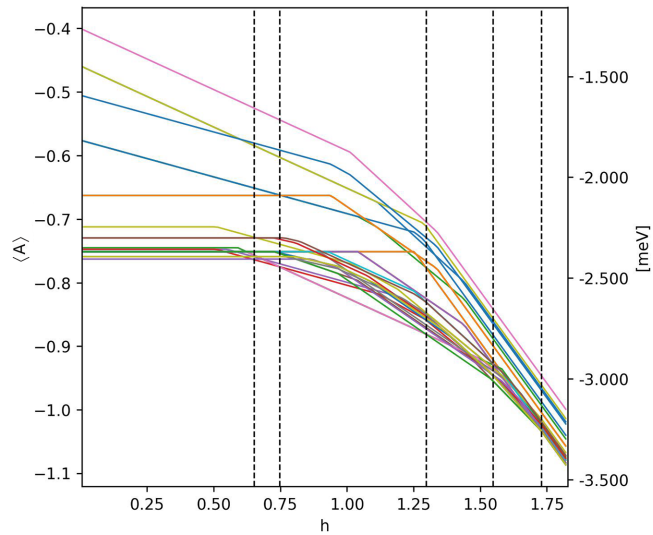

FIG. 8. Minimum average energy per Ho atom ($\langle A \rangle$) for all 33 acceptable magnetic unit cells for a magnetic field applied in the X direction. Dotted lines indicate phase transitions.

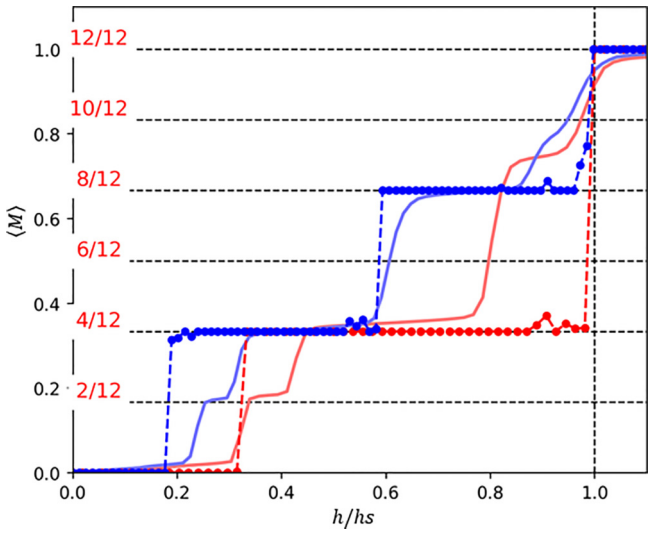

FIG. 9. Monte Carlo simulation of average Ho^{3+} magnetization as an external magnetic field is applied perpendicular (X, red) and parallel (Y, blue) to the easy axis calculated using empirical exchange parameters from Ref. [2] (dashed lines), compared to experiment [8].

transitions. This indicates that any further adjustment to the model would likely require either the introduction of further neighbor interactions, new interactions, or a search over a larger RCS.

Notably, this direct comparison of competing energy states cannot be done easily using a more standard Monte Carlo approach and further demonstrates the utility of this method.

C. Monte Carlo

Despite being systematic, a direct search of the reduced configuration space only applies to zero temperature and is limited in terms of the size of the magnetic unit cell. With this in mind, we have investigated the phase diagrams using Monte Carlo (MC) simulations. The classical dynamics of our model is adequately addressed with the Metropolis-Hastings algorithm and simulated annealing. The main challenge is that due to high frustration of our DFT-GF Hamiltonian the free energy landscape is crowded with metastable states; we mitigate this by a combination of annealing, aggressive averaging, and database bookkeeping of lowest-energy states.

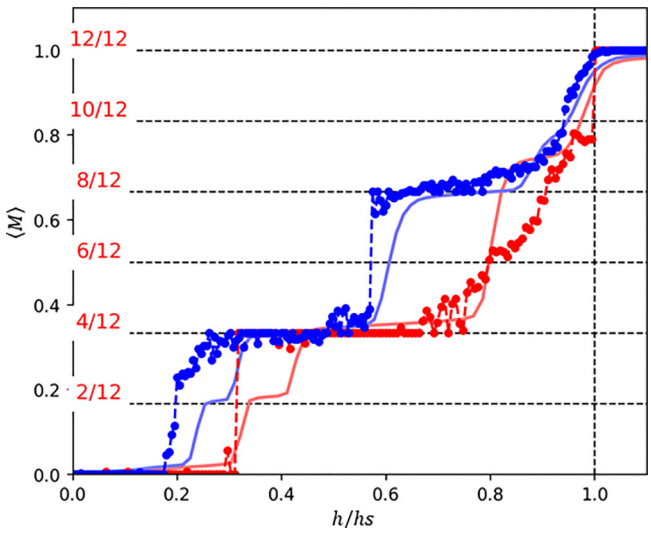

FIG. 10. Monte Carlo simulation of average Ho^{3+} magnetization as an external magnetic field is applied perpendicular (X, red) and parallel (Y, blue) to the easy axis calculated using DFT-GF first-principles exchange parameters (dashed lines), compared to experiment [8].

These MC simulations were performed on a periodic 18×18 lattice using the same annealing procedure at zero temperature for both the empirically found and the calculated parameters.

MC simulations using the empirical exchange parameters result in clear magnetization steps (Fig. 9) which match some, but not all, of the steps observed experimentally and are in agreement with the MC simulation reported in Refs. [2]. When using our first-principles parameters, which include J_5 bonds and distinguishing between J_{3a} and J_{3b} bonds, MC results in a less clear image of the magnetization plateaus (Fig. 10), but matches experimental observations far more closely for fields applied in both the X and Y directions [24]. Thus, the first-principles parameters pass the test of being relevant in the thermodynamic limit better than the empirical ones.

The noise present in the Monte Carlo simulations performed with our calculated parameters demonstrates how much more frustrated the system becomes with the inclusion of further neighbor interactions. To "smooth out" this noise would require exceedingly long simulations.

IV. CONCLUSIONS

By searching over a reduced configuration space for the minimum energy of differently shaped magnetic unit cells of the twisted kagome lattice and through the use of first-principles DFT-GF calculations to determine exchange parameters, we have been able to reproduce the magnetization plateaus observed in experimentation. We have also determined that the employment of larger magnetic unit cells and further neighbor interactions are crucial in reproducing the behavior observed in experiment.

In addition, we have shown the utility of a unique combination of approaches (DFT-GF and RCS search method) to a complicated system like HoAgGe twisted kagome, with advantages over more standard methods. We note that it is possible that the full phase diagram could be better captured using magnetic unit cells larger than six times the single unit cell volume [25]. Other limitations include even longer-range exchange interactions (HoAgGe being a metal, we expect the long-range exchange to be of Ruderman-Kittel-Kasuya-Yosida type, i.e., only cubically decaying) and deviations from the ideal Ising model.

ACKNOWLEDGMENTS

We are grateful to Nirmal Ghimire for attracting our attention to this compound, for sharing their experimental data, and for many useful discussions. This work was supported by the Office of Naval Research through Grant No. N00014-23-1-2480.

DATA AVAILABILITY

The data that support the findings of this article are not publicly available upon publication because it is not technically feasible and/or the cost of preparing, depositing, and hosting the data would be prohibitive within the terms of this research project. The data are available from the authors upon reasonable request.

[1] A. P. Ramirez, A. Hayashi, R. J. Cava, R. Siddharthan, and B. S. Shastry, Zero-point entropy in 'spin ice', Nature (London) **399**, 333 (1999).

[2] K. Zhao, H. Deng, H. Chen, K. A. Ross, V. Petříček, G. Günther, M. Russina, V. Hutanu, and P. Gegenwart, Realization of the kagome spin ice state in a frustrated intermetallic compound, Science **367**, 1218 (2020).

[3] M. Ezawa, Higher-order topological insulators and semimetals on the breathing kagome and pyrochlore lattices, Phys. Rev. Lett. **120**, 026801 (2018).

[4] M. Hering, F. Ferrari, A. Razpopov, I. I. Mazin, R. Valentí, H. O. Jeschke, and J. Reuther, Phase diagram of a distorted kagome antiferromagnet and application to Y-kapellasite, npj Comput. Mater. **8**, 10 (2022).

[5] J. Richter, J. Schulenburg, P. Tomczak, and P. Schmalfuß, The Heisenberg antiferromagnet on the square-kagome lattice, Condens. Matter Phys. **12**, 507 (2009).

[6] Y. N. Huang, H. O. Jeschke, and I. I. Mazin, CrRhAs: A member of a large family of metallic kagome antiferromagnets, npj Quantum Mater. **8**, 32 (2023).

[7] Y. Lee, R. Skomski, X. Wang, P. P. Orth, Y. Ren, B. Kang, A. K. Pathak, A. Kutepov, B. N. Harmon, R. J. McQueeney, I. I. Mazin, and L. Ke, Interplay between magnetism and band topology in the kagome magnets $R\mathrm{Mn}_6\mathrm{Sn}_6$, Phys. Rev. B **108**, 045132 (2023).

[8] H. Bhandari, P.-H. Chang, R. B. Regmi, B. G. Márkus, L. Forró, J. F. Mitchell, I. I. Mazin, and N. J. Ghimire, Tunable topological transitions in the frustrated magnet HoAgGe, Communications Materials **6**, 52 (2025).

[9] Y. Lee, Z. Ning, R. Flint, R. J. McQueeney, I. I. Mazin, and L. Ke, Toward a first-principles theory of rare-earth ions in crystals, npj Comput. Mater. **11**, 168 (2025).

[10] See Supplemental Material at http://link.aps.org/supplemental/10.1103/p8bq-9623 for additional phase diagrams, magnetization state plots, and validation of Ho easy axis calculations.

[11] P.-H. Chang and I. I. Mazin, Exploring metamagnetism in triangular Ising networks: Insights from further-neighbor interactions with a case study on ErGa_2, Phys. Rev. B **110**, 014418 (2024).

[12] T. Ozaki, Variationally optimized atomic orbitals for large-scale electronic structures, Phys. Rev. B **67**, 155108 (2003).

[13] Openmx, the code openmx pseudoatomic basis functions and pseudopotentials are available under terms of the GNU-GPL at http://www.openmx-square.org/.

[14] J. P. Perdew, K. Burke, and M. Ernzerhof, Generalized gradient approximation made simple, Phys. Rev. Lett. **77**, 3865 (1996).

[15] A. I. Liechtenstein, V. I. Anisimov, and J. Zaanen, Density-functional theory and strong interactions: Orbital ordering in Mott-Hubbard insulators, Phys. Rev. B **52**, R5467 (1995).

[16] S. L. Dudarev, G. A. Botton, S. Y. Savrasov, C. J. Humphreys, and A. P. Sutton, Electron-energy-loss spectra and the structural stability of nickel oxide: An LSDA+U study, Phys. Rev. B **57**, 1505 (1998).

[17] V. P. Antropov, M. I. Katsnelson, and A. I. Liechtenstein, Exchange interactions in magnets, Phys. B: Condens. Matter **237–238**, 336 (1997).

[18] M. I. Katsnelson and A. I. Lichtenstein, First-principles calculations of magnetic interactions in correlated systems, Phys. Rev. B **61**, 8906 (2000).

[19] A. Terasawa, M. Matsumoto, T. Ozaki, and Y. Gohda, Efficient algorithm based on Liechtenstein method for computing exchange coupling constants using localized basis set, J. Phys. Soc. Jpn. **88**, 114706 (2019).

[20] M. J. Han, T. Ozaki, and J. Yu, Electronic structure, magnetic interactions, and the role of ligands in Mn_n ($n = 4, 12$) single-molecule magnets, Phys. Rev. B **70**, 184421 (2004).

[21] These are the $0/1$, $1/5(x)$, $1/5(y)$, $1/3(x)$, $1/3(y)$, $1/2(x)$, $2/3(y)$, $3/4(x)$, $1/1(x)$, and $1/1(y)$ magnetization plateaus observed.

[22] At least three.

[23] J_{3a}, J_{3b}, J_4, and J_5 phase diagrams are shown in the Supplemental Material [10] and follow trends similar to those in the J_2 phase diagram.

[24] All Monte Carlo simulations across the different parameter sets were performed using the same simulation protocol.

[25] This was later confirmed using the GMU cluster computer, HOPPER, for magnetic unit cells of eight times the unit cell volume.